

TEMPERATURE INCREASE ASSOCIATED WITH PLASTIC DEFORMATION UNDER DYNAMIC COMPRESSION: APPLICATION TO ALUMINIUM ALLOY AL 6082

JOSÉ-LUIS PÉREZ-CASTELLANOS

*University Carlos III of Madrid, Department of Continuum Mechanics and Structural Analysis,
Madrid, Spain; e-mail: percaste@ing.uc3m.es*

ALEXIS RUSINEK

*National Engineering School of Metz (ENIM), Laboratory of Mechanics, Biomechanics, Polymers
and Structures (LaBPS), Metz, France; e-mail: rusinek@enim.fr*

The temperature increase associated with plastic deformation of a material under loading may be measured using several techniques such as infrared thermography (IRT). The present work investigates the temperature increase at different high strain rates and initial test temperatures, using an aluminium alloy Al 6082. A Split Hopkinson Pressure Bar (SHPB) was applied to induce high strain rates to the material and an infrared camera was used to measure the temperature increase. Numerical simulations of dynamic tests were performed to calculate the temperature increase and to gain a better understanding of the process by local measurements. Thus, a detailed finite-elements model was developed to simulate the dynamic compression test. The fraction of plastic work converted into heat was estimated using the Zehnder model. Numerical results in terms of the strain rate and initial temperature effect on the material temperature increase are reported and compared with experiments.

Key words: infrared thermography, plastic strain, adiabatic heating, Hopkinson bar

1. Introduction

Mechanical energy produced during plastic and elastic deformation of a metal is partially converted into heat while the rest is stored as deformation energy (Hodowany *et al.*, 1999; Kappor and Nemat-Nasser, 1998). This stored energy remains in the material after loading as internal defects, phase changes and

other permanent microstructural changes. The heat generated, proportional to a part of the mechanical work, induces a temperature increase of the material.

The thermal-balance equation for a visco-plastic isotropic material is given by Eq. (1.1). It does not consider the effect related to phase-transformation processes in the heat generation as discussed in Rusinek and Klepaczko (2009)

$$\lambda \nabla^2 T - \dot{T} = -\frac{\beta}{\rho C_P} \boldsymbol{\sigma} : \dot{\boldsymbol{\epsilon}}^p + \frac{\alpha}{\rho C_P} \frac{E}{1-2\nu} T \operatorname{tr}(\dot{\boldsymbol{\epsilon}}^e) \quad (1.1)$$

where λ is the thermal diffusivity of the material, T is the absolute temperature, β is the Quinney-Taylor coefficient (Taylor and Quinney, 1934), (proportion of plastic-deformation energy converted into heat), ρ is the mass density, C_P is the specific heat, $\boldsymbol{\sigma}$ is the stress tensor, $\dot{\boldsymbol{\epsilon}}^p$ is the plastic strain-rate tensor, $\dot{\boldsymbol{\epsilon}}^e$ is the elastic-strain-rate tensor, α is the thermal-expansion coefficient, ν is Poisson's ratio, and E is Young's modulus.

Close to 10 s^{-1} for metals (Klepaczko *et al.*, 2009; Oussouaddi and Klepaczko, 1991; Rusinek and Klepaczko, 2001; Rusinek *et al.*, 2007) no heat is exchanged with the surroundings, and adiabatic conditions may be assumed $\lambda \nabla^2 T = 0$. If thermoelasticity is not considered, then the temperature increase ΔT , may be calculated as a function of the plastic strain $\bar{\boldsymbol{\epsilon}}^p$

$$\Delta T(\bar{\boldsymbol{\epsilon}}^p) = \int_0^{\bar{\boldsymbol{\epsilon}}_{max}^p} \frac{\beta}{\rho C_P} \bar{\sigma}(\bar{\boldsymbol{\epsilon}}^p) d\bar{\boldsymbol{\epsilon}}^p \quad (1.2)$$

where $\bar{\sigma}$ is the equivalent stress under uniaxial deformation and $\bar{\boldsymbol{\epsilon}}^p$ is the corresponding equivalent plastic strain.

It is usual to consider β as constant in such calculations. Nevertheless, it is accepted that β depends on the plastic strain. Different models (Aravas *et al.*, 1990; Rosakis *et al.*, 2000; Zehnder, 1991) to define the Quinney-Taylor coefficient β , have been developed. Based on the Zehnder model, related to the calculation of stored energy by unit of dislocation density, the Quinney-Taylor coefficient β , may be defined as below

$$\beta(\bar{\boldsymbol{\epsilon}}^p) \approx 1 - \left. \frac{\partial \bar{\sigma}(\bar{\boldsymbol{\epsilon}}^p)}{\partial \bar{\boldsymbol{\epsilon}}^p} \frac{1}{E} \right|_{\bar{\boldsymbol{\epsilon}}^p} \quad (1.3)$$

where E is material Young's modulus.

If a potential hardening law is used (which allows an isotropic behaviour to be defined while considering just hardening), an analytical expression for the

Quinney-Taylor coefficient $\beta(\bar{\varepsilon}^p)$, Eq. (1.4), may be defined (Zehnder, 1991) from Eq. (1.3)

$$\beta(\bar{\varepsilon}^p) = 1 - n \left(\frac{\bar{\varepsilon}^p}{\varepsilon_0} \right)^{n-1} \quad (1.4)$$

where ε_0 is the yield strain and n is the hardening exponent of the material. The temperature increase in a specimen deformed during plastic deformation may be calculated using Eq. (1.2) and Eq. (1.4).

There are at least two procedures for measuring the temperature increase ΔT associated with the plastic strain $\bar{\varepsilon}^p$. The first one is based on the use of a rapid-response thermocouple connected to the specimen tested. The second one is based on the measurement of the thermal radiation of the specimen emitted during deformation. It corresponds to the temperature field observed on the surface of the material.

The IRT technique has been widely used to correlate plastic strain to temperature increase $\Delta T(\bar{\varepsilon}^p)$ in metal and polymeric materials. This technique is steadily more used due to the development of new high-speed infrared cameras. During the last decade, several authors were using the IRT technique to estimate the temperature increase of materials during elastic and plastic deformation. For example, Kappor and Nemat-Nasser (1998), Manson *et al.* (1994), Rabin and Rittel (2000) measured the temperature increase under dynamic compression tests using a SHPB device. Chrysochoos and Louche (2000) applied thermographic analysis to the deformation process of Polymethyl-methacrylate (PMMA). Trojanowski *et al.* (1998) used IRT to investigate the heat generation in an epoxy resin and in metal specimens, coupled to a SHPB. Titanium-alloy specimens were tested by Macdougall and Harding (1998), using a split Hopkinson torsion and tensile bars and by using an infrared radiometer to measure the temperature increase during the test. The IRT technique to investigate impact processes of steels at high strain rates was used by Guduru *et al.* (2001), Rusinek *et al.* (2003), and Rodríguez-Martínez *et al.* (2010).

The objective of the present study is to investigate the temperature increase ΔT associated with the plastic strain $\bar{\varepsilon}^p$ at high strain rates $\dot{\bar{\varepsilon}}^p$ using an aluminium alloy Al 6082. The technique used to measure the temperature increase is based on the IRT. Concerning the mechanical loading, a SHPB is used to reach high strain rates under dynamic compression. Coupling the SHPB and IRT technique, it allows the temperature increase ΔT to be defined and estimated at high strain rates during plastic deformation $\Delta T(\bar{\varepsilon}^p, \dot{\bar{\varepsilon}}^p)$.

For the test simulation, a detailed numerical model of the SHPB test was developed using a FE code. With this 3D model, extensive numerical analyses were made to calculate the temperature increase and other local quantities to

compare with the experiments. This kind of technique using coupling experiments and simulations, steadily more used, is called the “Inverse Method”. It allows one to reach local quantities to complement measurements of macroscopic behaviour made during experiments, for a better understanding of the material behaviour (Rusinek *et al.*, 2008; Miguélez *et al.*, 2009).

2. Test description

Guzmán *et al.* (2009), and Pérez-Castellanos *et al.* (2010) have developed an original set-up and a SHPB testing procedure with a simultaneous measurement of the temperature increase $\Delta T(\bar{\varepsilon}^p, \dot{\bar{\varepsilon}}^p)$, using an infrared camera (IRC) and the dynamic mechanical behaviour of the material $\bar{\sigma}(\bar{\varepsilon}^p, \dot{\bar{\varepsilon}}^p, T)$. The next part of the paper provides a detailed description of the technique used.

2.1. Test set-up

For dynamic testing, a SHPB was used. This device, developed originally by Kolsky (1949) consists of two coaxial bars between which the specimen is fixed. A cylindrical striker of the same material and with the same cross-sectional area as the bars is launched, using a pneumatic gas gun, to impact against the incident bar. As a result of the impact, a compressive square-shaped pulse travels through the incident bar until it reaches the specimen; the magnitude of the incident wave is $\sigma_i = \rho C V_0 / 2$ with a duration of $t_p = 2L_p / C$. In the previous formulas, ρ is the bar density of the material; C is the elastic wave speed, which depends on Young’s modulus E ; with $C = \sqrt{E/\rho}$; V_0 is the velocity of the striker just before impact, and L_p is the striker length. When the incident wave ε_i reaches the incident bar-specimen interface, it is split into reflected ε_r , and transmitted waves ε_t . Two strain gauges, on full bridge, fixed on the incident bar and the transmitter bar, respectively, allow recording of the elastic strain waves. The strains are related to the stress quantities using Hooke’s law.

The temperature increase during the test is measured using an IRC with a temperature resolution of 20 mK. The frequency acquisition of the camera may be increased by reducing the frame size (subwindow mode). A subwindow of 64x16 pixels was used, thus achieving 3290 frames per second, with an acquisition time of 40 μ s (T_{ACQ}). Before starting the tests, the camera was calibrated using a black body from 273 K to 373 K.

The specimen is placed in a test chamber to isolate it from spurious external radiation. Thus the IRC measures only thermal radiation. Inside the chamber, there are electrical resistances controlled by thermocouples with which the specimen may be heated until reaching the defined test temperature. The maximum temperature allowable is 573 K.

A dark chamber is placed between the test chamber and the IRC. This chamber was designed taking into account the working focal distance of the IRC.

Figure 1a shows a picture of the test chamber and the dark chamber connected to the Hopkinson bar. Figure 1b shows a picture inside the test chamber with the electrical resistances to enable the test to be performed at different initial temperatures.

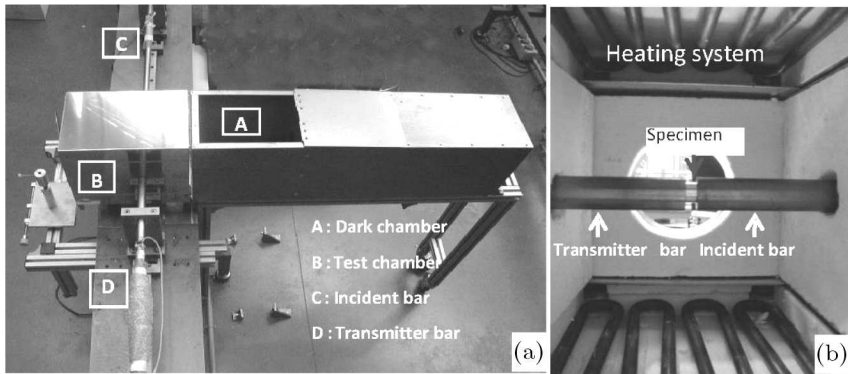


Fig. 1. (a) Coupled SHPB, test chamber, and dark chamber, (b) internal test-chamber description

A fundamental aspect of the testing system is the synchronism between the SHPB and the IRC. This synchronism is achieved by means of a trigger system. The synchronization system consists of two photoelectric sensors, two optical fibres, and a time counter. During experiments, the photo-sensors detect the striker arrival and generate a trigger signal. By the use of this synchronization system, it is possible to associate the temperature measured by the IRC with a value of the strain in the specimen during the deformation process.

2.2. Test procedure

The test procedure is based on the classical SHPB testing methodology. The main difference is that several mechanical and electronic time intervals must be controlled to ensure synchronism between the SHPB and the IRC, allowing a better analysis on time of the signals.

The strain rate $\dot{\varepsilon}$ imposed on the specimen depends on the striker velocity V_0 and is proportional to the air pressure stored in the gas gun chamber and to the specimen length L_o . The nominal strain ε_N , the strain rate $\dot{\varepsilon}_N$, and the nominal stress σ_N , imposed on the material may be calculated with knowledge of the incident wave ε_i , the reflected wave ε_r , and the transmitted wave ε_t , recorded, using the following expressions, Eq. (2.1). This is based on the theory of one-dimensional elastic-wave analysis while assuming mechanical-force equilibrium of the specimen

$$\begin{aligned}\varepsilon_N(t) &= \frac{2C}{L_o} \int_0^t \varepsilon_r(\tau) d\tau & \dot{\varepsilon}_N(t) &= \frac{2C}{L_o} \varepsilon_r(t) \\ \sigma_N(t) &= E \frac{A}{A_S} \varepsilon_t(t)\end{aligned}\tag{2.1}$$

where C is the velocity of the elastic waves, A_S is the initial cross section of the specimen, A is the cross section of the bar, L_o is the initial length of the specimen, and E is the Young modulus of the bar material. The true stress $\bar{\sigma}$, and true strain $\bar{\varepsilon}$, may be calculated, respectively, using the following expressions, Eq. (2.2), and assuming plasticity with constant volume $\nu = 0.5$

$$\bar{\sigma} = \sigma(1 - \varepsilon_N) \quad \bar{\varepsilon} = -\ln(1 - \varepsilon_N)\tag{2.2}$$

The physical process of temperature measurement by the IRC is described as follows. The IRC receives and measures the outgoing radiance from the object R_{out} . This radiance has two components: the emitted R_{emi} , and the reflected R_{ref} . The emitted radiance may be calculated as $R_{emi} = \epsilon R_0(T_{emi})$ where $R_0(T_{emi})$ is the radiance emitted by the black body for the same specimen temperature T_{emi} , and ϵ is the specimen-surface emissivity factor. The reflected radiance may be calculated as $R_{ref} = r R_0(T_{amb})$ where $R_0(T_{amb})$ is the radiance emitted by the black body at room temperature T_{amb} , and r the specimen-surface reflectance ($r = 1 - \epsilon$). The radiance received and measured by the IRC is related to its emitted and reflected components as

$$R_{out} = \epsilon R_0(T_{emi}) + (1 - \epsilon) R_0(T_{amb})\tag{2.3}$$

R_{out} is measured using the IRC, $R_0(T_{amb})$ may be calculated using the well-known Planck's law expression, and ϵ must be firstly estimated. From these parameters, $R_0(T_{emi})$ may be calculated using Eq. (2.3). Finally, the temperature of the specimen T may be deduced as the value at which the integral of the Planck law expression $R_0(\lambda, T)$, over the spectral range of the camera, equals to $R_0(T_{emi})$.

The IRC records the radiation during an exposure interval $[t_{FR}, t_{FR} + T_{ACQ}]$ where t_{FR} is the time when the frame recording starts and T_{ACQ} is the acquisition time. From the recorded radiation, a temperature value is determined. This temperature is associated with the middle point, $t_{FR} + T_{ACQ}/2$, of the exposure interval to relate it with the plastic strain, using the synchronism system.

In each test, a set of successive IR images was also recorded by the IRC. The images were processed to draw a temperature map and a temperature profile along a generatrix line (ΔT vs. pixel). This temperature profile includes the specimen and one segment of each bar (incident and transmitter) on both sides of the specimen with a total length equal to the horizontal dimension of the window used (64×16 pixels), Fig. 1b and Fig. 3.

The frame rate of the camera used does not allow more than two or three temperature measurements during the complete loading time. Therefore, to have more values of the temperature increase, several tests must be performed for the same initial conditions. Thus, the temperature-increase value $\Delta T(\bar{\varepsilon}^p, \dot{\bar{\varepsilon}}^p)$ for a set of initial conditions, was calculated using an average quantity $\overline{\Delta T} = N^{-1} \sum_1^N \Delta T_{test}$ where N is the number of tests performed.

3. Results and discussion

3.1. Material

The material used in this study is an aluminium alloy Al 6082 (Mrówka-Nowotnik and Sieniawski, 2005; Mann *et al.*, 2007; Manping *et al.*, 2008; Agena, 2009; Dadbakhsh *et al.*, 2010). This alloy is a medium-strength structural alloy that includes in its chemical composition 0.7-1.3 Si, 0.4-1.0 Mn, 0.6-1.2 Mg and 0.4-0.15 Cr; the manganese controls the grain structure and size. Depending of the manganese added, this alloy has high values of mechanical properties and is used for industrial application where both lightness and high strength are required. In Table 1, the mechanical static parameters characterizing our alloy Al 6082 are reported.

Table 1. Mechanical parameters of alloy Al 6082

Tensile strength [MPa]	Yield stress [MPa]	Elongation [%]	Young's modulus [GPa]
300-320	280	13	69.5

The material was supplied in the form of extruded bars and machined to the final geometry: 7.0 mm long and 14 mm in diameter inducing a ratio

$s_0 = h_0/d_0 = 0.5$. The specimens previously underwent a process of polishing and a lubricant (MoS_2) was used to reduce the friction effect μ between the specimen and the bars. The friction effect is related to the parameter s_0 as reported in Malinowski and Klepaczko (1986), and Jankowiak *et al.* (2011). All the specimens before the tests were covered with soot to increase the material-emissivity factor ϵ .

The value of the material-emissivity factor ϵ was calculated experimentally. A specimen was heated on the heating plate from room temperature to 393 K. During the heating process, the temperature time course was measured simultaneously by the IRC and by a thermocouple fixed on the specimen. The two temperature measurements were compared to determine the emissivity-factor value ϵ of the material considered. With the use of this technique, the average of the emissivity factor was estimated to $\epsilon = 0.8$.

3.2. Experimental results

Several compression tests were performed at room temperature, 293 K, for different strain rates. The reproducibility of the tests was verified by comparing several results under the same experimental conditions. Thus the results in terms of $\bar{\sigma} - \bar{\epsilon}^p$ and $\Delta T - \bar{\epsilon}^p$ curves for the same set of experimental conditions were consistent with a maximum difference of 1% for an imposed condition in terms of the strain rate and initial temperature.

Figure 2 shows, as an example, the true stress/true plastic-strain relationship that resulted at room temperature and different strain rates varying from $300 \text{ s}^{-1} \leq \dot{\bar{\epsilon}}^p \leq 1500 \text{ s}^{-1}$.

From the true-stress/true-strain curves, the logarithmic strain-rate-sensitivity coefficient was calculated, $m = (\partial \log \sigma / \partial \log \dot{\epsilon})|_{\epsilon, T} = 0.03$, which may be considered as a moderate value in the interval of the strain rates tested. Nevertheless, remarkable temperature sensitivity of this alloy is noted, $\nu = (\partial \log \sigma / \partial \log T)|_{\epsilon, \dot{\epsilon}} = -0.4$.

Figure 3 shows, as an example, several profiles of temperature increase that resulted during the tests at room temperature for a strain rate of $\dot{\epsilon} = 600 \text{ s}^{-1}$. Each profile shows a relatively constant temperature value with two peaks corresponding to the perimeter of the circular bases of the specimens. These peaks are due to the friction effect inducing an additional temperature increase and, therefore, not considered to represent the temperature increases in the specimen.

Table 2 presents the results of the measured temperature increase including the initial temperature T_0 the average strain rate reached during the test $\dot{\bar{\epsilon}}^p$,

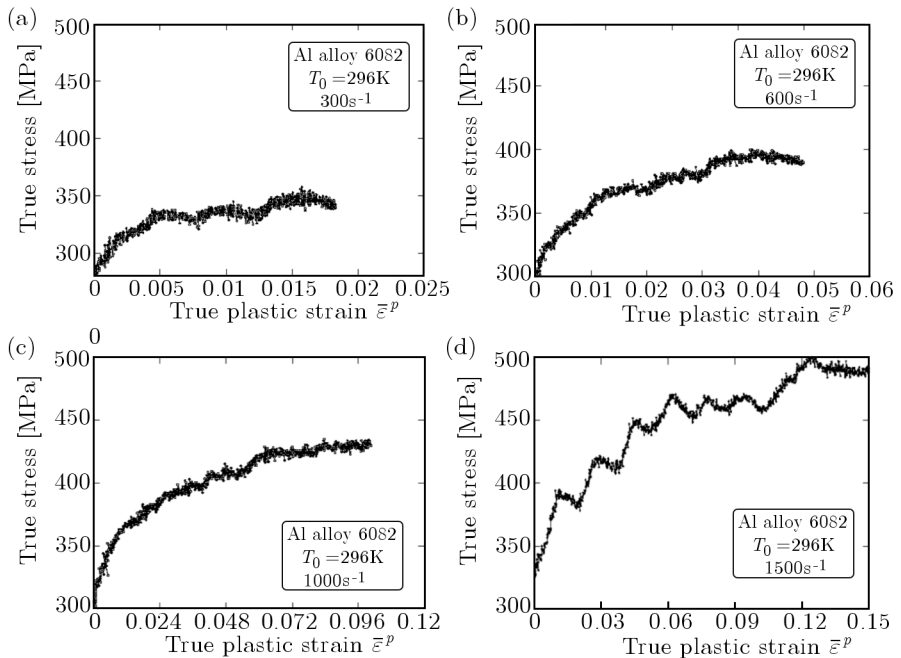


Fig. 2. $\bar{\sigma} - \bar{\epsilon}^p$ curves for Al 6082 alloy at room temperature; (a) $\dot{\bar{\epsilon}}^p = 300\text{ s}^{-1}$, (b) $\dot{\bar{\epsilon}}^p = 600\text{ s}^{-1}$, (c) $\dot{\bar{\epsilon}}^p = 1000\text{ s}^{-1}$ and (d) $\dot{\bar{\epsilon}}^p = 1500\text{ s}^{-1}$

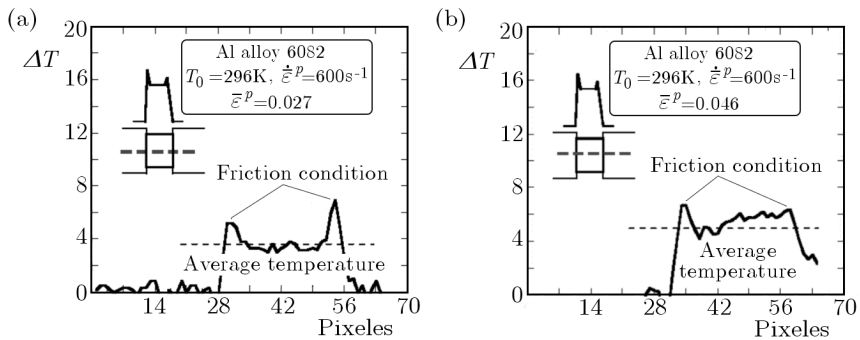


Fig. 3. Profiles of temperature increase corresponding to different strain levels at room temperature and strain rate $\dot{\bar{\epsilon}}^p = 600\text{ s}^{-1}$; (a) $\bar{\epsilon}^p = 0.027$ and (b) $\bar{\epsilon}^p = 0.046$

the plastic strain level $\bar{\epsilon}^p$, and the associated recorded temperature increase under dynamic compression ΔT .

From the previous values, Table 2, it is observed that $\Delta T(\bar{\epsilon}^p)$ did not depend on the strain rate for an imposed strain level and initial temperature; this is due to a reduced strain-rate sensitivity of the alloy Al 6082, as discussed previously.

Table 2. Tests results: test temperature T_0 , plastic strain rate reached $\dot{\bar{\epsilon}}^p$, plastic strain $\bar{\epsilon}^p$ and the associated temperature increment ΔT

T_0 [K]	$\dot{\bar{\epsilon}}^p$ [s ⁻¹]	$\bar{\epsilon}^p$ [-]	ΔT [K]
296	600	0.014	1.4
	600	0.027	3.0
	600	0.046	5.8
296	1000	0.026	3.1
	1000	0.047	6.1
	1000	0.07	9.7
	1000	0.092	13
373	1500	0.038	3.5
	1500	0.127	15
	1500	0.195	20

Immediately after the process of plastic deformation ended, a small temperature decrease was detected. This temperature decrease was due to the elastic recovery as observed precisely under a quasi-static compression test. The load applied to the specimen consisted of a periodic compression force with an amplitude of 32.3 kN and a frequency of 0.185 Hz. This load amplitude corresponds to a material-stress level of $\sigma_{loading} = 210$ MPa, which is less than the material yield stress. The frequency value was chosen to be able to reproduce it on the test machine.

Figure 4 shows the loading force vs. time and the temperature increase vs. time relations.

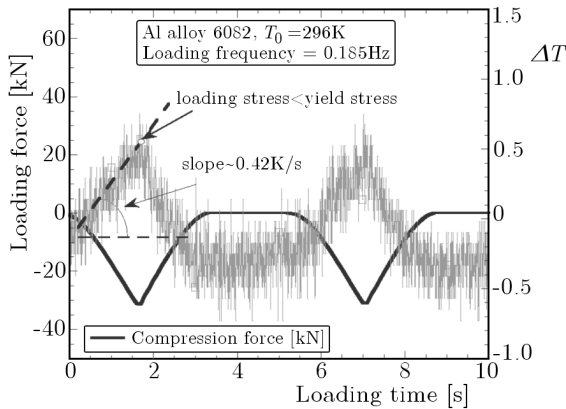


Fig. 4. Loading force vs. time and temperature vs. time relations measured during the experiment

The maximum temperature increase was found to be close to 0.5 K. It was also observed that the decreasing slope defines a temperature decrease of the same magnitude as the thermal expansion parameter of the material. The temperature increase, $\Delta T(\bar{\varepsilon}^p, \dot{\bar{\varepsilon}}^p)$, corresponds to a rate of 0.42 K/s. This rate corresponds exactly to the rate calculated using the analytical expression derived by Thomson (1853), which is the last term of Eq. (1.1) and representing the temperature variation associated with the elastic strain, Eq. (3.1).

The temperature increase, as elastic recovery, proved to be of the same order of magnitude, close 0.5 K. Thus, the temperature decrease observed at the end of the test may be considered to correspond to the elastic recovery process.

3.3. Numerical analyses

A three-dimensional finite-element model was used to simulate the SHPB tests. The commercial finite-element code ABAQUS/Explicit, 2006, was used to investigate the precise thermo-mechanical process in the specimen under dynamic loading and the phenomenon of elastic-wave propagation. The FEM model developed is described in the following sections.

3.3.1. Model description

The model includes the two elastic bars, the striker, and the specimen using real dimensions (incident and transmitter bars 1 m long with a diameter of 22 mm and for the striker a length of 330 mm with the same bar diameter; Fig. 5).

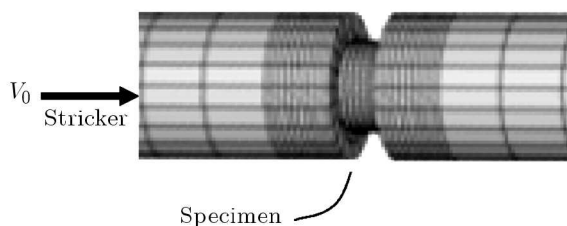


Fig. 5. 3D finite element model of SHPB test

The specimen and bars are free of movement along the bars axis. The radial movement of the nodes on the model axis is restricted.

The mesh of the incident bar, the transmitter bar, the specimen, and the striker were made using hexahedral elements with 8 nodes, C3D8R (ABAQUS/Explicit, 2006), reproducing the total geometry of the device. The

density of the mesh directly influences two fundamental factors of the analysis: the accuracy of the solution reached and the time of calculations. Therefore, it is necessary to achieve a balance between these two variables. The study of the sensitivity of the mesh was carried out before beginning the numerical analyses considering just the incident and the transmitter bars.

Several numerical models with FE meshes with 18 320 to 34 508 elements were considered. On the first time, a comparison was made of the incident ε_i , the reflected ε_r , and the transmitted ε_t waves calculated using these different numerical models. It was found that there is no strong variation between the wave profiles and level calculated (Fig. 6). On the second time, the temperature increase on the specimen surface calculated using these numerical models were also compared; as a result, minor influence of the mesh density on the temperature increase (in the interval of elements number considered) was deduced. Thus, the density of 18 320 elements was considered optimal.

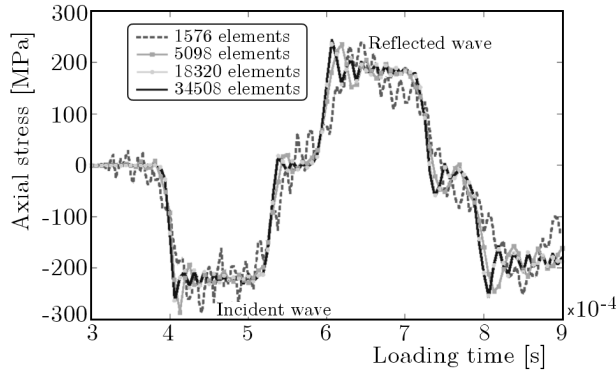


Fig. 6. Analysis of the mesh-sensitivity of the SHPB model using only the transmitter bar

The contact conditions between the surfaces of the striker-incident bar, incident-bar specimen, and specimen-transmitter bar were taken into account. The tangential interaction between the contact surfaces can be established by means of Coulomb's friction law.

Based on the Klepaczko and Malinowski model (Malinowski and Klepaczko, 1986), additional energy for a deformation range is observed depending on the specimen ratio used during the tests. This energy, related to friction, induces an extra stress increase; the stress level will change, increasing with the friction coefficient. Thus, the stress level measured includes material behaviour and friction effects. To correct the latter, the model proposes the expression

$$\mu(\bar{\varepsilon}) = \frac{\bar{\sigma} - \bar{\sigma}_0}{\bar{\sigma}} 3s_0 [\exp(\bar{\varepsilon})]^{\frac{3}{2}} \quad (3.1)$$

where $\bar{\sigma}$ is the compressive true stress, $\bar{\sigma}_0$ is the compressive true stress determined for an ideal test without friction specimen/bars, $s_0 = h_0/d_0$ is the ratio between the initial specimen height and diameter, and $\bar{\varepsilon}$ is the true strain.

The Klepaczko and Malinowski model has some limits and may be used as an average range of μ varying from 0 to 0.25. A recent complete analysis of this model is reported in Jankowiak *et al.* (2011).

An experimental characterization of the friction coefficient $\mu(\bar{\varepsilon})$ was carried out using the Klepaczko and Malinowski model. Figures 7a and 7b show the relation between μ and $\bar{\varepsilon}$ calculated for a strain rate of 300 s^{-1} and 600 s^{-1} , respectively. It can be seen that μ remains more or less constant and equal to 0.09. This value of friction coefficient was the one used during numerical calculations (the same for all test conditions) and implies no contact.

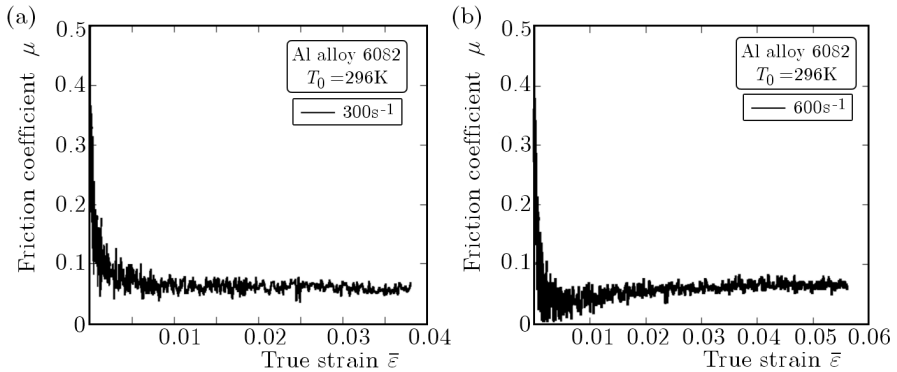


Fig. 7. Relations $\mu - \bar{\varepsilon}$ for different strain rates under dynamic compression, Eq. (3.1)

During the experiments, the striker velocity V_0 just before impact, was measured with two fibre-optic photoelectric sensors. This velocity was used during numerical simulations as the initial boundary condition. The wave transmission through the bars occurs after the impact, and the incident, reflected, and transmitted waves can be calculated along the mesh, and more precisely, for a distance corresponding to it where the strain gauges are glued along the bars.

The material of the incident and transmitter bars is an Inconel steel: Young's modulus equal to 211 GPa and Poisson's ratio equal to 0.3; the density considered is equal to 8190 kg/m^3 . The material of the striker is steel: Young's modulus equal to 207 GPa and Poisson's ratio of 0.3; the density considered is 7800 kg/m^3 .

To describe behaviour of the isotropic alloy Al 6082, the J_2 theory was assumed to define the flow stress. The elastic constants were defined from the corresponding experimental test. The hardening function considered was

defined using the Johnson-Cook model, Eq. (3.2), since the material exhibits a low strain-rate dependency (frequently reported for aluminium 6082). This model is well defined to describe this kind of material behaviour (linear strain rate sensitivity)

$$\begin{aligned}\bar{\sigma}(\bar{\epsilon}^p, \dot{\bar{\epsilon}}^p, T) &= [A + B(\bar{\epsilon}^p)^n] \left(1 + C \ln \frac{\dot{\bar{\epsilon}}^p}{\dot{\bar{\epsilon}}_0}\right) (1 - T^{*m}) \quad \rightarrow \quad \dot{\bar{\epsilon}}^p \geq \dot{\bar{\epsilon}}_0 \\ \bar{\sigma}(\bar{\epsilon}^p, T) &= [A + B(\bar{\epsilon}^p)^n] (1 - T^{*m}) \quad \rightarrow \quad \dot{\bar{\epsilon}}^p < \dot{\bar{\epsilon}}_0\end{aligned}\quad (3.2)$$

with

$$T^* = \frac{T - T_{room}}{T_{melt} - T_{room}}$$

where $\bar{\sigma}$ is the equivalent stress, $\bar{\epsilon}^p$ is the equivalent plastic strain, $\dot{\bar{\epsilon}}^p$ is the equivalent plastic strain rate, $\dot{\bar{\epsilon}}_0$ is the reference strain rate, T_{melt} is the melting temperature, and T_{room} is the room temperature. As material parameters, A is the initial yield stress, B is the hardening modulus, n is the hardening exponent, C is the coefficient of strain rate sensitivity, and m is the temperature sensitivity exponent.

The parameters A , B , C , n , and m were calculated by applying the root-mean-square method coupled to Eq. (3.2) and based on experimental true stress/plastic strain curves obtained at 296 K for $\dot{\bar{\epsilon}}^p = 300 \text{ s}^{-1}$, at 296 K for $\dot{\bar{\epsilon}}^p = 1000 \text{ s}^{-1}$ and at 373 K for $\dot{\bar{\epsilon}}^p = 1500 \text{ s}^{-1}$. Figure 8 shows the experimental true stress/plastic strain curve obtained at 296 K for $\dot{\bar{\epsilon}}^p = 600 \text{ s}^{-1}$ and the corresponding true stress/plastic strain curve using the values calculated for parameters A , B , C , n , and m . A good agreement was found between the experiments and numerical results.

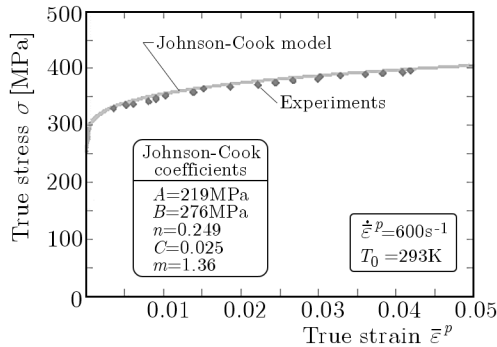


Fig. 8. Experimental and $J - C$ true stress-plastic strain curves for a test at 296 K and $\dot{\bar{\epsilon}}^p = 600 \text{ s}^{-1}$

Non-constant values of the Quinney-Taylor coefficient β were considered. The previous relation proposed by Zehnder, Eq. (1.4), is valid for materials

showing a strain/energy transformed into heat dependency as alloy Al 6082 in this experiment. The temperature increase ΔT , measured during the tests at room temperature $T_0 = 296$ K, and for a plastic-strain value $\bar{\varepsilon}^p = 0.027$, can be determined from Table 2, these values being $\Delta T = 3$ K for $\dot{\bar{\varepsilon}}^p = 600$ s⁻¹ and $\Delta T = 3.2$ K (extrapolated from $\bar{\varepsilon}^p = 0.026$) for $\dot{\bar{\varepsilon}}^p = 1000$ s⁻¹. Both temperature-increase values are practically equal, and thus it can be deduced that the proportion of plastic work converted into heat β does not depend on the strain rate for alloy Al 6082.

Nevertheless, no conclusions can be drawn with respect to the dependency of β on temperature because the mechanical behaviour of alloy Al 6082 depends heavily on temperature. The variation of the temperature increase ΔT associated with plastic strain is due to mainly the aforementioned dependency.

These results lead to the conclusion that the use of the Zehnder model is appropriate in this case, since the tested material is not strain-rate dependent as reported before.

The temporal evolution of the stress-strain state of the system was analysed by direct integration of the equations of motion and the constitutive equations. The implicit algorithm proposed by Zaera and Fernández-Sáez (2006) was used to integrate the Johnson-Cook constitutive equation. This algorithm was modified to include the dependency of β on $\bar{\varepsilon}^p$, Eq. (1.4).

For the validation of the numerical model proposed, the experimental and the analytical elastic waves were compared. Figure 9 shows the experimental and numerical incident, reflected and transmitted nominal stress waves; the three waves verify the relation

$$\varepsilon_I + \varepsilon_R = \varepsilon_T \quad (3.3)$$

A good agreement between the experiments and numerical results was found.

The radial-nominal stress component is also plotted in Fig. 9. It can be seen that the values of this wave are practically negligible, allowing for the fulfilment of the hypothesis of negligible radial inertia during the SHPB test due to the initial shape geometry (Malinowski and Klepaczko, 1986).

3.3.2. Results

Figure 10 shows the relations $\bar{\sigma} - \bar{\varepsilon}^p$ found during the numerical analyses at room temperature and a strain rate of 300 s⁻¹, 600 s⁻¹, and 1000 s⁻¹, together with the $\beta - \bar{\varepsilon}^p$ relations calculated using Eq. (1.4). It may be observed that the usual hypothesis taking β as constant is, in this case, available for high plastic-strain values. The medium value calculated for β was 0.9, which is similar to that currently used for metal alloys.

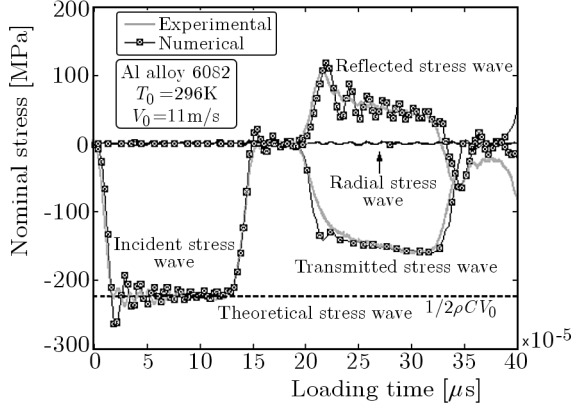


Fig. 9. Incident, reflected and transmitted longitudinal-nominal stress waves and radial-nominal stress wave

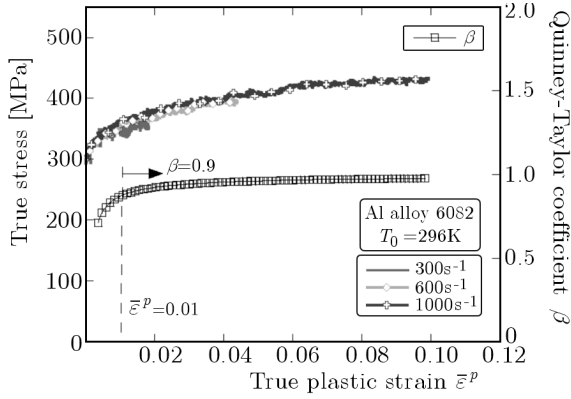


Fig. 10. Relations $\bar{\sigma} - \bar{\epsilon}^p$ and $\beta - \bar{\epsilon}^p$ for different dynamic strain rates at room temperature

Figures 11a and 11b show, respectively, a map of the plastic deformation and the temperature increase for calculation time of $t = 120 \mu\text{s}$, initial temperature of 296 K and a strain rate of $\dot{\bar{\epsilon}}^p = 1000 \text{ s}^{-1}$.

The cylindrical surface of the specimen shows uniform fields of plastic deformation (Fig. 11a and temperature Fig. 11b). It is observed using numerical simulations that on the specimen bases, local increments of plastic deformation and temperature take place as observed during experiments using IR temperature measurements. These local increments are related to friction effects between the specimen and the bars. Localized small non-symmetrical irregularities are also noticed; these irregularities are due to the non-exact cylindrical symmetry of the mesh. A temperature increase on the specimen

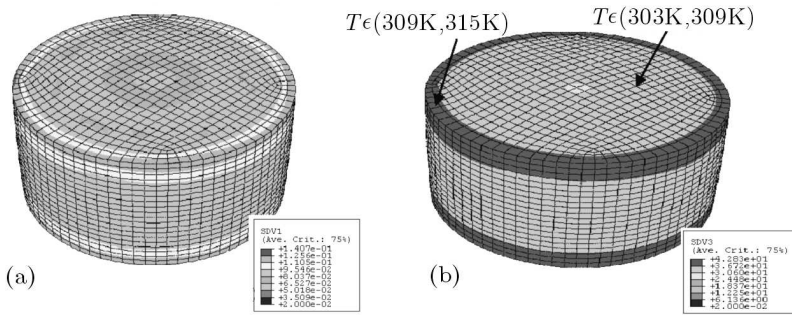


Fig. 11. (a) Plastic strain and (b) temperature maps resulting from numerical simulation at room temperature for a strain rate $\dot{\epsilon}^p = 1000\text{ s}^{-1}$ and corresponding to a plastic strain value $\bar{\epsilon}^p = 0.07$

surface (initial test temperature equal to 296 K) between 7 K and 13 K can be seen. This value is of the same order as the one measured during the experiments (Table 2).

Figure 12 gives the numerical (continuous line) and experimental (symbol) temperature profiles along a generatrix line taken on the surface of the deformed specimen. The numerical profile corresponds to the temperature map using Fig, 11b. The two profiles discussed above show a good agreement. The temperature increase at the contact between the bars and specimen was higher than the temperature increase in the specimen middle zone, due to friction effects. The difference in the central zone is due to a possible variation of the soot coating due to its ejection during experiments.

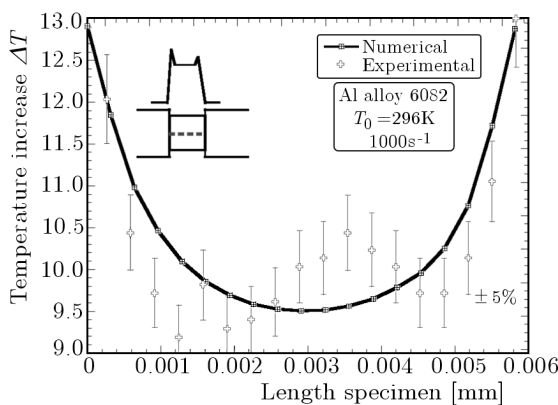


Fig. 12. Experimental and numerical temperature profiles for an imposed strain level under dynamic compression and corresponding to a strain level of $\bar{\epsilon}^p = 0.07$

As a result of numerical simulations, the temperature increments of the specimen surface were calculated and compared with the experimental results. Figure 13 shows the temperature evolution during the plastic-deformation process for two different strain rates using numerical simulations. The simulated tests were at $\dot{\bar{\epsilon}}^p = 600 \text{ s}^{-1}$ and $\dot{\bar{\epsilon}}^p = 1000 \text{ s}^{-1}$, both at room temperature, and at 373 K and $\dot{\bar{\epsilon}}^p = 1500 \text{ s}^{-1}$. Figure 13 also plots the experimental temperature-increase values associated with the corresponding plastic-strain values (Table 2).

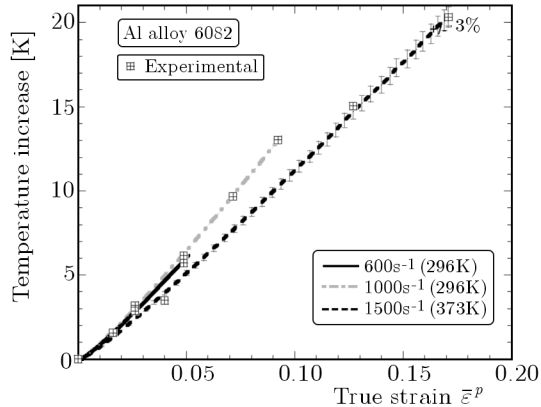


Fig. 13. Numerical and experimental $T - \bar{\epsilon}^p$ results for different strain rates under dynamic compression

A good agreement is observed between the experiments and numerical simulations in terms of the temperature increase ΔT for the strain-rates and test temperature considered.

4. Conclusions

By an experimental procedure developed, the temperature increase associated with plastic deformation during SHPB tests was measured for an Al alloy 6082.

The results of the tests reveal that the temperature increases with the strain rate and decreases when the initial test temperature is higher.

At the final deformation stage, a minor temperature decrease occurs, presumably associated with an elastic unloading process.

A three-dimensional numerical model of the SHPB test including the incident bar, transmitter bar, the projectile and the specimen was developed.

The Zehnder model was linked to an implicit integration algorithm and implemented as a user subroutine in the commercial finite-elements code ABAQUS/Explicit. This model offers a prediction in terms of temperature increase associated with plastic deformation.

The results validated the applicability of Zehnder's expression to model the proportion of plastic-deformation energy transformed into heat β for materials that are strain dependent and strain rate non-dependent. Nevertheless, no conclusions could be drawn with respect to the dependency of β on temperature.

A good agreement was found between the experimental and numerical results, providing a better understanding of experimental measurement using an inverse method.

Acknowledgements

The author from UC3M thanks Dr. Rolando Guzmán López for his collaboration, interest and discussions.

References

1. AGENA A.S.M., 2009, A study of flow characteristics of nanostructured Al-6082 alloy produced by ECAP under upsetting test, *J. of Mater. Proc Tech.*, **209**, 2, 856-863
2. ARAVAS N., KIM K.S., LECKIE F.A., 1990, On the calculations of the stored energy of cold work, *J. Eng. Mater. Technol.*, **112**, 4, 465-470
3. CHRYSOCHOOS A., LOUCHE H., 2000, An infrared image processing to analyse the calorific effects accompanying strain localisation, *Int. J. Eng. Sci.*, **38**, 1759-1788
4. DADBAKHS S., KARIMI TAHERI A., SMITH C.W., 2010, Strengthening study on 6082 Al alloy after combination of aging treatment and ECAP process, *Mater. Sci. and Eng.: A*, **527**, 18/19, 4758-4766
5. GUDURU P.R., ROSAKIS A.J., RAVICHANDRAN G., 2001, Dynamic shear bands: an investigation using high speed optical and infrared diagnostics, *Mechanics of Material*, **33**, 371-402
6. GUZMÁN R., ESSA Y.E., MELÉNDEZ J., ARANDA J., LÓPEZ F., PÉREZ-CASTELLANOS J.L., 2009, Measurement of temperature increment in compressive quasi-static and dynamic tests using the infrared thermography, *Strain*, **45**, 2, 179-189

7. HODOWANY J., RAVICHANDRAN G., ROSAKIS A.J., ROSAKIS P., 1999, Partition of plastic work into heat and stored energy in metals, *Experimental Mechanics*, **40**, 113-123
8. JANKOWIAK T., RUSINEK A., LODYGOWSKI T., 2011, Validation of the Klepaczko-Malinowski model for friction correction and recommendations on split Hopkinson pressure bar, *Finite Elements in Analysis and Design*, **47**, 10, 1191-1208
9. KAPPOR R., NEMAT-NASSER S., 1998, Determination of temperature rise during high strain rate deformation, *Mechanics of Material*, **27**, 1-12
10. KARLSSON AND SORENSEN, INC., 2006, Abaqus, v6.4 User's Manual
11. KLEPACZKO J.R., RUSINEK A., RODRÍGUEZ-MARTÍNEZ J.A., PECHERSKI R.B, ARIAS A., 2009, Modeling of thermo-viscoplastic behaviour of DH-36 and Weldox 460-E structural steels at wide ranges of strain rates and temperatures, comparison of constitutive relations for impact problems, *Mechanics of Material*, **41**, 599-621
12. KOLSKY H., 1949, An investigation of the mechanical properties of materials at very high rates of loading, *Proc. Phys. Soc.*, **B62**, 676-699
13. MACDOUGALL D., HARDING J., 1998, The measurement of specimen surface temperature in high-speed tension and torsion test, *Int. J. of Impact Engin.*, **21**, 6, 473-488
14. MALINOWSKI J.Z., KLEPACZKO J.R., 1986, A unified analytic and numerical approach to specimen behaviour in the Split-Hopkinson pressure bar, *Int. J. Mech. Sci.*, **28**, 6, 381-391
15. MANN T., HÄRKEGÅRD G., STÄRK K., 2007, Short fatigue crack growth in aluminium alloy 6082-T6, *Int. J. of Fatigue*, **29**, 8/11, 1820-1826
16. MANPING L., HANS J.R., YINGDA Y., JENS C.W., 2008, Deformation structures in 6082 aluminium alloy after severe plastic deformation by equal-channel angular pressing, *Mater. Sci. and Eng., A*, **483/484**, 59-63
17. MANSON J.J., ROSAKIS A.J., RAVICHANDRAN, 1994, On the strain and strain rate dependence of the fraction of plastic work converted to heat: an experimental study using high speed infrared detectors and the Kolsky bar, *Mechanics of Material*, **17**, 135-145
18. MIGUELEZ M.H., ZAERA R., MOLINARI A., CHERIGUENE R., RUSINEK A., 2009, Residual stresses in orthogonal cutting of metals: The effect of thermo-mechanical coupling parameters and of friction, *Journal of Thermal Stresses*, **32**, 269-289
19. MRÓWKA-NOWOTNIK G., SIENIAWSKI J., 2005, Influence of heat treatment on the microstructure and mechanical properties of 6005 and 6082 aluminium alloys, *J. of Mater. Proc. Tech.*, **162/163**, 367-372

20. OUSSOUADDI O., KLEPACZKO J.R., 1991, An analysis of transition from isothermal to adiabatic deformation in the case of a tube under torsion, *Proceedings of the conference on DYMAT 91. J. Phys. IV*; Coll. C3 (Suppl. III): C3-C323
21. PÉREZ-CASTELLANOS J.L., GUZMÁN R., RUSINEK A., MELÉNDEZ J., 2010, Temperature increment during quasi-static compression tests using Mg metallic alloys, *Materials and Design*, **31**, 7, 3259-3269
22. RABIN Y., RITTEL, D., 2000, Infrared temperature sensing of mechanically loaded specimens: thermal analysis, *Experimental Mechanics*, **40**, 197-202
23. RODRÍGUEZ-MARTÍNEZ J.A., RUSINEK A., CHEVRIER P., BERNIER R., ARIAS A., 2010, Temperature measurements on ES steel sheets subjected to perforation by hemispherical projectiles, *Int. J. Impact. Eng.*, **37**, 828-841
24. ROSAKIS P., ROSAKIS A.J., RAVICHANDRAN G., HODOWANY J., 2000, A thermodynamic internal variable model for the partition of plastic work into heat and stored energy in metals, *Journal Mech. Phys. Solids*, **48**, 581-607
25. RUSINEK A., KLEPACZKO J.R., 2001, Effect of adiabatic heating in some processes of plastic deformation, *4th International Symposium on Impact Engineering*, Kunamoto, Japán, *Impact Engineering and Application*, **I/II**, 37-53
26. RUSINEK A., NOWACKI W.K., GADAJ P., KLEPACZKO J.R., 2003, Measurement of temperature coupling by thermovision and constitutive relation at high strain rates for the dual phase sheet steel, *Journal de Physique IV France*, **110**, 411-416
27. RUSINEK A., KLEPACZKO J.R., 2007, Experiments on heat generated during plastic deformation and stored energy for TRIP steels, *Materials and Design*, **30**, 35-48
28. RUSINEK A., ZAERA R., KLEPACZKO J.R., 2007, Constitutive relations in 3-D for a wide range of strain rates and temperatures – application to mild steels, *Int. J Solids Structures*, **44**, 5611-5634
29. RUSINEK A., CHERIGUENE R., BAUMER A., KLEPACZKO J.R., LAROUR P., 2008, Dynamic behaviour of high-strength sheet steel in dynamic tension, experimental and numerical analyses, *Journal of Strain Analysis for Engineering Design*, **43**, 37-53
30. TAYLOR G.I., QUINNEY M.A., 1934, The latent energy remaining in a metal after cold working, *Proc. R. Soc. London*, **A143**, 307-326
31. THOMSON W. (LORD KELVIN), 1853, On dynamical theory of heat, *Trans. R. Soc. Edimb.*, 261-282
32. TROJANOWSKI A., MACDOUGALL D., HARDING J., 1998, An improved technique for the experimental measurement of specimen surface temperature during Hopkinson-bar tests, *Measurement Sci. Tech.*, **9**, 12-19

33. ZAERA R., FERNÁNDEZ-SÁEZ J., 2006, An implicit consistent algorithm for the integration of thermoviscoplastic constitutive equations in adiabatic conditions and finite deformations, *International Journal of Solids and Structures*, **43**, 6, 1594-1612
34. ZEHNDER A.T., 1991, A model for the heating due to plastic work, *Mechanics Research Communications*, **18**, 1, 23-28

Wzrost temperatury wywołany plastycznym odkształceniem przy dynamicznym ściskaniu – analiza stopu aluminium Al 6082

Streszczenie

Wzrost temperatury w materiale związany z plastycznym odkształcaniem może być rejestrowany różnymi metodami, w tym m.in. techniką termografii podczerwieni (IRT). Prezentowana praca poświęcona jest badaniom wzrostu temperatury przy różnym tempie odkształceń i temperatury początkowej próbek wykonanych ze stopu aluminium Al 6082. W eksperymentach użyto zmodyfikowanego pręta Hopkinsona do generowania szybko-zmiennych odkształceń w materiale i jednocześnie dokonywano pomiarów temperatury za pomocą kamery termowizyjnej. Przeprowadzono także symulacje numeryczne przebiegu przyrostu temperatury pozwalające na lepsze zrozumienie zachodzących procesów na podstawie lokalnych pomiarów. W tym celu zbudowano szczegółowy model bazujący na metodzie elementów skończonych, który przeanalizowano pod kątem dynamicznego ściskania. Część pracy odkształcenia plastycznego zamienianego w ciepło oszacowano za pomocą modelu Zehndera. Wyniki obliczeń uwzględniających tempo odkształceń i temperaturę początkową na jej przyrost w badanym materiale zweryfikowano z rezultatami doświadczeń.

Manuscript received April 15, 2011; accepted for print July 7, 2011